ACADEMIC PRESS

Available online at www.sciencedirect.com
SCIENCE DIRECT®

Journal of Catalysis 217 (2003) 141–151

JOURNAL OF CATALYSIS

www.elsevier.com/locate/jcat

Preparation and heterogeneous photocatalytic behaviors of the surface-modified porous silica materials impregnated with monosubstituted keggin units

Yihang Guo,[a] Changwen Hu,[a,b,*] Chunjie Jiang,[a] Yu Yang,[a] Shicheng Jiang,[a] Xiliang Li,[a] and Enbo Wang [a]

[a] *Faculty of Chemistry, Northeast Normal University, Changchun, 130024, People's Republic of China*
[b] *Chemistry of Department, Beijing Institute of Technology, Beijing, 100081, People's Republic of China*

Received 8 October 2002; revised 6 January 2003; accepted 8 January 2003

Abstract

Amine-functionalized mesoporous and macroporous silica materials impregnated with transition-metal-monosubstituted polyoxometalate $K_6[Ni(H_2O)SiW_{11}O_{39}]$ ($SiW_{11}Ni$) clusters were prepared by coordination of nickel centers in the cluster with the amine surface groups in silica supports. The structures and compositions of the materials were characterized by UV–vis diffuse reflectance spectra (DR-UV–vis), infrared (IR) spectra, and ^{29}Si MAS NMR, indicating that the $SiW_{11}Ni$ clusters were chemically attached to the silica supports, and the primary Keggin structure remained intact in the as-synthesized composites. The topologies and porosities of the materials were characterized by scanning electron microscopy (SEM), transmission electron microscopy (TEM), and nitrogen adsorption determination. The heterogeneous photocatalytic behaviors of the materials were tested via degradation of dye rhodamine B (RB), and a RB degradation mechanism was proposed based on the detected intermediates and final products. That is, photocatalytic degradation of RB on the supported $SiW_{11}Ni$ underwent the successive steps of deethylation, deamination, decarboxylation, and cleavage of the chromophore ring structure, resulting in the final products of CO_2, NO_3^-, and Cl^- ions. A Drop of $SiW_{11}Ni$ clusters from the amine-modified silica matrix into the reaction system was hardly observed during the photocatalytic tests, attributed to the strong coordination interaction between the $SiW_{11}Ni$ molecule and the amine-modified silica support.

Keywords: Polyoxometalate; Porous materials; Heterogeneous photocatalysis; Dye; Rhodamine B

1. Introduction

The photochemical, electrochromic, and magnetic properties of polyoxometalates (POMs) significantly impact the development of materials with these properties, and some applications of POMs include stains electron microscopy, catalysts, and ion-exchange materials [1–5]. Soluble POM catalysts can catalyze a large variety of reaction types but suffer from their inability to be recycled [6–8]. Moreover, the specific surface areas of solid POMs are low (< 10 m^2/g [8]), leading to very few active sites on their surfaces. Thus, immobilization of POMs onto solids to create hybrid catalysts is necessary for recovery and possibly recyclability. At the same time, their catalytic activities are expected to be improved. In our previous works we prepared a series of insoluble POM-containing hybrid catalysts by attachment of POM to the porous inorganic solids via acid–base interactions or covalent bond formation [9–11]. In these hybrid materials, the inorganic precursors used were free acids of saturated Keggin units, decatungstate, and monovacant Keggin-type units. We also investigated the heterogeneous photocatalytic behaviors of these supported POM catalysts via degradation of organic pollutants in aqueous solutions. It is found that the catalytic activity of POM in the hybrid catalyst is improved significantly due to the fascinating physical and chemical properties and unusual internal surface topology of the porous materials, and separation and recovery of the POM from the reaction environment became easy.

For catalytic applications, aminopropyl-functionalized silica materials are the most widely studied organic-inorga-

* Corresponding author.
E-mail address: huchw@nenu.edu.cn (C. Hu).

0021-9517/03/$ – see front matter
doi:10.1016/S0021-9517(03)00037-X

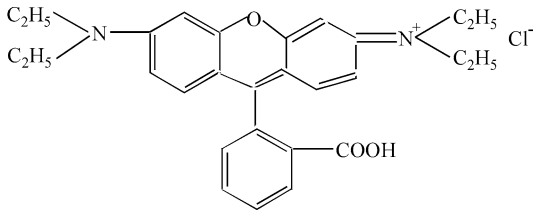

Scheme 1. Chemical structure of Rhodamine B.

nic hybrid solids [12]. Here, we designed and prepared a series of new solid POM catalysts by using 3-aminopropyltriethoxysilane ($(EtO)_3SiCH_2CH_2CH_2NH_2$, APS)-functionalized porous silica materials as the supports, and transition-metal-substituted polyoxometalate (TMSP) clusters were used as the active sites. This design was based on the structure characteristic of TMSP; that is, TMSPs are considered to be inorganic porphyrins [13–20], large inert ligands, which leave accessible coordination sites on the transition metal center. In these "inorganic porphyrins," the lacunary POM coordinates the transition metal with five O^{2-} ligands, while the last coordinate site on the metal is occupied by an aqua ligand. The aqua ligand of most TMSPs can be displaced in aqueous media by ligands such as pyridines or ammonia [19,20]. Therefore, TMSP was attached onto the surface of APS-silica via coordination bond formation.

Dyes are important organic pollutants, and their release as wastewater in the ecosystem is a dramatic source of esthetic pollution, eutrophication, and perturbations in aquatic life [21–24]. Most of the dyes are resistant to biodegradation and direct photolysis, and many N-containing dyes such as RB undergo natural reductive anaerobic degradation to yield potentially carcinogenic aromatic amines. In the present work, the catalytic behaviors of the as-synthesized porous $SiW_{11}Ni$–APS–SiO_2 composites were tested via heterogeneous photocatalytic oxidation of aqueous RB (the chemical structure of RB is shown in Scheme 1). In addition, the photocatalytic activities of the $SiW_{11}Ni$–APS–SiO_2 composites were also compared with pure $SiW_{11}Ni$ (in homogeneous systems) and microporous $SiW_{11}Ni/SiO_2$ prepared via the sol–gel method. Lastly, the mechanism of RB photodegradation over the as-synthesized porous $SiW_{11}Ni$ composites was proposed via careful analysis of the RB degradation intermediates and final products identified through electrospray mass spectrometer (ES-MS) and ion chromatograph (IC). Meanwhile, the changes of color in the reaction system were directly related to the structure change of the RB chromophore, which is helpful in understanding the RB photodegradation mechanism over the as-synthesized porous $SiW_{11}Ni$ composites.

2. Methods

2.1. Materials

Mesoporous silica supports such as SIO-5, SIO-6, and SIO-7 are commercially available and supplied by the Catalysis Society of Japan. Another mesoporous silica support was prepared in the current experiment (see below). Monodisperse polystyrene (PS) latex spheres were synthesized in an emulsifier-free emulsion, which was reported in our previous work [11]. APS (AR) was purchased from J & Kchemica Inc., Beijing, China. The following reagents were all AR grade, purchased from Beijing, China: tetraethyl orthosilicate (TEOS), $Na_2WO_4 \cdot 2H_2O$, $NiSO_4 \cdot 6H_2O$, potassium acetate, acetic acid, ethanol (EtOH), 1-butanol (1-BuOH), and nitric acid. Doubly distilled water was used in all experiments. The preparation of $K_6[Ni(H_2O)SiW_{11}O_{39}]$ was adapted from the literature methods [25].

2.2. Catalyst preparation

Microporous $SiW_{11}Ni/SiO_2$ composite was prepared via the sol–gel method at pH 3.5, following our previous work [9,10], and the $SiW_{11}Ni/H_2O/TEOS/1$-BuOH molar ratio was 1/2000/1920/272.

Mesoporous silica support was also prepared by the sol–gel method at pH 1.0, and the method is similar to that of the microporous $SiW_{11}Ni/SiO_2$ except that no $SiW_{11}Ni$ was added, and the $H_2O/TEOS/1$-BuOH molar ratio was 10.4/1/1.42.

Macroporous silica support was prepared by the sol–gel (pH 1) as well as templating techniques (PS spheres were used as the template), which is similar to our method for preparation of macroporous $[X^{n+}W_{11}O_{39}]^{(12-n)-}$–$SiO_2$ composites except that no $[X^{n+}W_{11}O_{39}]^{(12-n)-}$ was added [11], and the $H_2O/TEOS/1$-BuOH molar ratio was 11.6/4.4/1.

The preparation of amine-modified porous silica supports (APS–SiO_2 or APS–SIO) was as described below. The dried silica support (1 g) was dispersed in 50 ml of toluene. To this was added 1.5 g of APS. The mixture was stirred vigorously at room temperature for 12 h while reflux was used, and then the products (APS–SiO_2, APS–SIO-5, APS–SIO-6, APS–SIO-7, and macroporous APS–SiO_2, respectively) were recovered by centrifugation.

The preparation of porous amine-modified silica materials impregnated with $SiW_{11}Ni$ ($SiW_{11}Ni$–APS–SiO_2 or $SiW_{11}Ni$–APS–SIO) was as described below. Amined-modified silica support (0.25 g) was dispersed in an aqueous $SiW_{11}Ni$ solution (0.125 g of $SiW_{11}Ni$ and 25 ml of water). The acidity of the mixture was controlled at pH 6–7. The mixture was stirred for 24 h at room temperature, centrifuged, washed with water, and dried to obtain $SiW_{11}Ni$-impregnated silica composites.

2.3. Characterization

Elemental analyses were performed on a Leeman Plasma Spec (I) ICP-AES and P-E 2400 CHN elemental analyzer. DR-UV–vis and FT-IR spectra were recorded on a Cary 500 UV-VIS-NIR spectrophotometer and a Nicolet Magna 560

IR spectrophotometer, respectively. ^{29}Si MAS NMR spectra were obtained on a Varian Unity-400 NMR spectrometer. SEM micrographs were obtained on a Hitachi S-570 scanning electron microscope, and TEM micrographs were obtained on a Hitachi H-7500 transmission electron microcsope. BET specific surface areas, pore sizes, and pore volumes were calculated from nitrogen adsorption isotherms determined at −196 °C using an ASAP 2010M surface analyzer (the samples were outgassed under vacuum at 200 °C).

2.4. Photocatalytic testing

The photoreactor was designed with a cylindrical quartz cell configuration and an internal light source surrounded by a quartz jacket, where the suspension of the catalyst and an aqueous RB completely surrounded the light source. The temperature of the suspension was maintained at 20 ± 2 °C by water circulation through an external cooling coil. The optical pathlength was ca. 2 cm. The light source was a 125 W high-pressure mercury lamp (HPML; output mainly at 313.2 nm).

The general photocatalytic procedure was carried out as follows. The catalyst (containing 30 mg of pure $SiW_{11}Ni$ in each of $SiW_{11}Ni$-impregnated silica composites) was suspended in a fresh aqueous RB solution (50 mg L^{-1} or 0.10 mmol L^{-1}). The suspension (80 ml) was ultrasonicated for 10 min and stirred in the dark for 30 min to obtain a good dispersion and adsorption. The lamp was inserted into the suspension after its intensity became stable. The suspension was vigorously stirred with the photoreactor open to air during the process.

After the reaction finished, the suspensions were centrifuged. Decreases of the RB concentrations were monitored via spectrophotometry. Changes of the concentrations of the intermediates and final products were analyzed by a DX-300 IC equipped with a conductivity detector. A CS12 cation column was used for determination of NH_4^+ ions; an AS4A anion column was used for determination of NO_2^- and NO_3^- ions; an ICE-ASI anion column was used for determinations of organic acids. Other highly polar and less volatile intermediate products in aqueous solution were identified by LCQ ES-MS.

3. Results and discussion

3.1. Preparation and characterization of the porous amine-modified silica materials impregnated with $SiW_{11}Ni$ clusters

The goal of the present work is the preparation of a new type of porous POM photocatalytic material. In this material, POM clusters were attached onto the surface of the supports through chemical but not physical interactions; therefore, dropping of the POM clusters from the supports can be controlled effectively. On the basis of this idea, we first modified the porous silica supports by propylamine groups to their surface silanol groups [26,27], and then $SiW_{11}Ni$ was chemically anchored to the amine-modified silica surface through Ni–N dative bonding; this preparation pathway is presented in Scheme 2. Attachment of the $SiW_{11}Ni$ cluster into the APS–SiO_2(SIO) support is very easy. In the $SiW_{11}Ni$ cluster, the coordinating interaction between nickel atom and aqua ligand is weak, and this coordinate site on nickel atoms can easily be displaced by some ligands such as ammonia via formation of a new coordinate bond. Here, meso- and macroporous $SiW_{11}Ni$–APS–SiO_2(SIO) composites were formed via coordination of nickel centers in the cluster with the amine surface groups in silica supports while mixing $SiW_{11}Ni$ and APS–SiO_2(SIO) at pH 6–7 (this acidity can ensure no degradation of $SiW_{11}Ni$ and no decomposition of propylamine groups).

The determined amounts of attached APS and $SiW_{11}Ni$ on different supports are presented in Table 1. It indicated

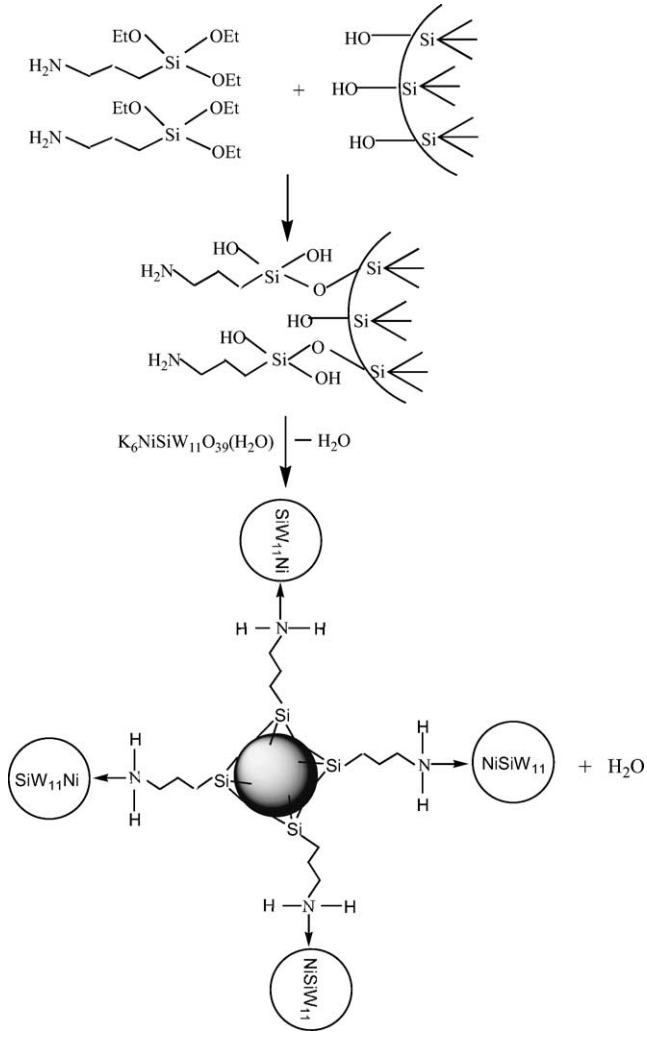

Scheme 2. Pathway of preparation of amine-modified silica attached with $SiW_{11}Ni$, where the black ball represents silica network. $SiW_{11}Ni$ and silica are bonded by coordination of nickel centers in the cluster with the nitrogen atom of amine surface groups in modified silica.

Table 1
Data (%) of elemental analyses for the starting $SiW_{11}Ni$ and their corresponding porous composites

Sample	Si	W	Ni	K	N
$SiW_{11}Ni$ (found)	0.94	67.3	2.06	7.72	–
$SiW_{11}Ni$ (calculated)	0.93	67.7	1.98	7.84	–
Microporous $SiW_{11}Ni/SiO_2$	–[a]	26.4	0.81	3.03	
Mesoporous $SiW_{11}Ni$–APS–SiO_2	–[a]	10.5	0.30	1.22	2.05
Mesoporous $SiW_{11}Ni$–APS–SiO-5	–[a]	19.8	0.63	2.30	1.82
Mesoporous $SiW_{11}Ni$–APS–SiO-6	–[a]	22.5	0.60	2.61	1.95
Mesoporous $SiW_{11}Ni$–APS–SiO-7	–[a]	35.1	1.02	4.07	1.78
Macroporous $SiW_{11}Ni$–APS–SiO_2	–[a]	25.1	0.73	2.91	1.18

[a] Content of Si in the TMSP–APS–SiO_2 composites cannot be determined accurately because the samples were digested with HF and HNO_3 before ICP-AES determination.

Table 2
Surface textural properties of the silica supports and their corresponding $SiW_{11}Ni$-containing porous composites

Sample	Surface area ($m^2\ g^{-1}$)	Average pore diameter (nm)	Pore volume ($cm^3\ g^{-1}$)
Microporous $SiW_{11}Ni/SiO_2$	385.6	0.65	0.38
Mesoporous SiO_2 (sol–gel)	237.8	3.80	0.22
Mesoporous $SiW_{11}Ni$–APS–SiO_2	196.3	2.71	0.20
SIO-5	192.0	15.6	0.36
Mesoporous $SiW_{11}Ni$–APS–SiO-5	169.3	14.1	0.34
SIO-6	109.0	29.5	0.46
Mesoporous $SiW_{11}Ni$–APS–SiO-6	83.7	27.3	0.43
SIO-7	82.0	46.2	0.42
Mesoporous $SiW_{11}Ni$–APS–SiO-7	73.9	42.6	0.39
Macroporous SiO_2	97.3	2.80	0.26
Macroporous $SiW_{11}Ni$–APS–SiO_2	91.6	1.20	0.11

that the APS/silica ratio is mainly dependent on the specific surface areas of the silica supports used (Table 2); e.g., N loading for mesoporous $SiW_{11}Ni$–APS–SiO_2 is the highest, while it is the lowest for the macroporous $SiW_{11}Ni$–APS–SiO_2. The explanation is that large specific surface area resulted in a higher number of surface hydroxyl groups available, therefore, a large number of propylamine groups were grafted to the silica surface via Si–O–Si linkage. The determined Ni/W atomic ratios for the $SiW_{11}Ni$–APS–SiO_2(SIO) composites were close to those of the cluster precursor. As for the mesoporous $SiW_{11}Ni$–APS–SiO_2(SIO), the larger the pore size, the higher the $SiW_{11}Ni$ loading obtained. The reason is that lager pore sizes are favored for anchoring large Keggin units [$SiW_{11}Ni$].

$SiW_{11}Ni$–APS–SiO_2(SIO) materials prepared in the current work exhibited all the features of the original coordinated $SiW_{11}Ni$ cluster in the DR-UV–vis (Fig. 1), FT-IR (Fig. 2), and ^{29}Si MAS NMR. First, five $SiW_{11}Ni$–APS–SiO_2(SIO) and microporous $SiW_{11}Ni/SiO_2$ composites all exhibit UV–vis absorption maximum at ca. 200, 260, 413, and 700 nm, respectively, which are in agreement with the starting $SiW_{11}Ni$. Absorptions at 200 and 260 nm are attributed to charge transfer from an O^{2-} ion to a W^{6+} ion in $SiW_{11}Ni$ cluster at W=O and W–O–W bonds, respectively, corresponding to higher absorption intensity (Fig. 1A). Absorptions at 413 and 700 nm originate from a d–d transition typical for octahedral Ni^{2+} with six oxygen bond ligands. This d–d transition corresponds to weaker absorption intensity (Fig. 1B). Pure $SiW_{11}Ni$ compounds display a characteristic infrared fingerprint (Fig. 2A) in the region of ca. 1000 to 700 cm^{-1} [28], attributed to the stretching vibrations of the Si–O (998 cm^{-1}) bond in the central SiO_4 unit, W=O (955 cm^{-1}), and W–O–W (905, 797, and 703 cm^{-1}) bonds of the cluster, respectively. These characteristic IR absorption data are very useful for identifying the structures of $SiW_{11}Ni$ compounds. In cases of pure $SiW_{11}Ni$ or microporous $SiW_{11}Ni/SiO_2$ (Fig. 2B), absorption at ca. 3445 cm^{-1} is due to the vibration of hydroxyl groups in the aqua ligand of the cluster or surface hydroxyl groups (Si–OH) of the silica support. As for the $SiW_{11}Ni$–APS–SiO_2(SIO) composites, their IR data (Figs. 2C–2F) first confirmed that the propylamine groups were attached onto the surface of the porous silica supports, i.e., absorption peaks appearing at 3430 to 3440 cm^{-1} were mainly attributed to the vibrations of N–H bonds, and the surface hydroxyl groups on the silica supports also disturbed this kind of vibration by forma-

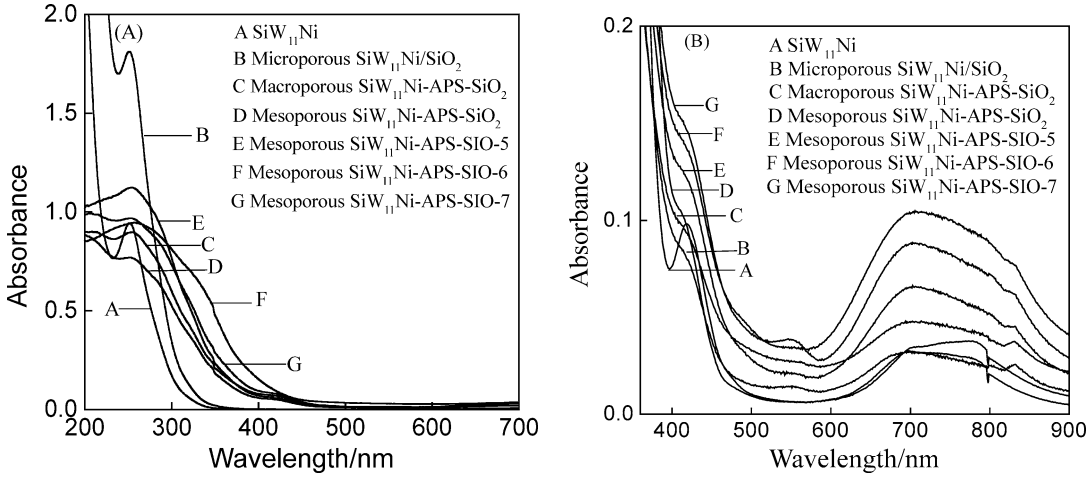

Fig. 1. DR-UV (A) and DR-VIS (B) spectra of the starting $SiW_{11}Ni$ and their corresponding porous materials.

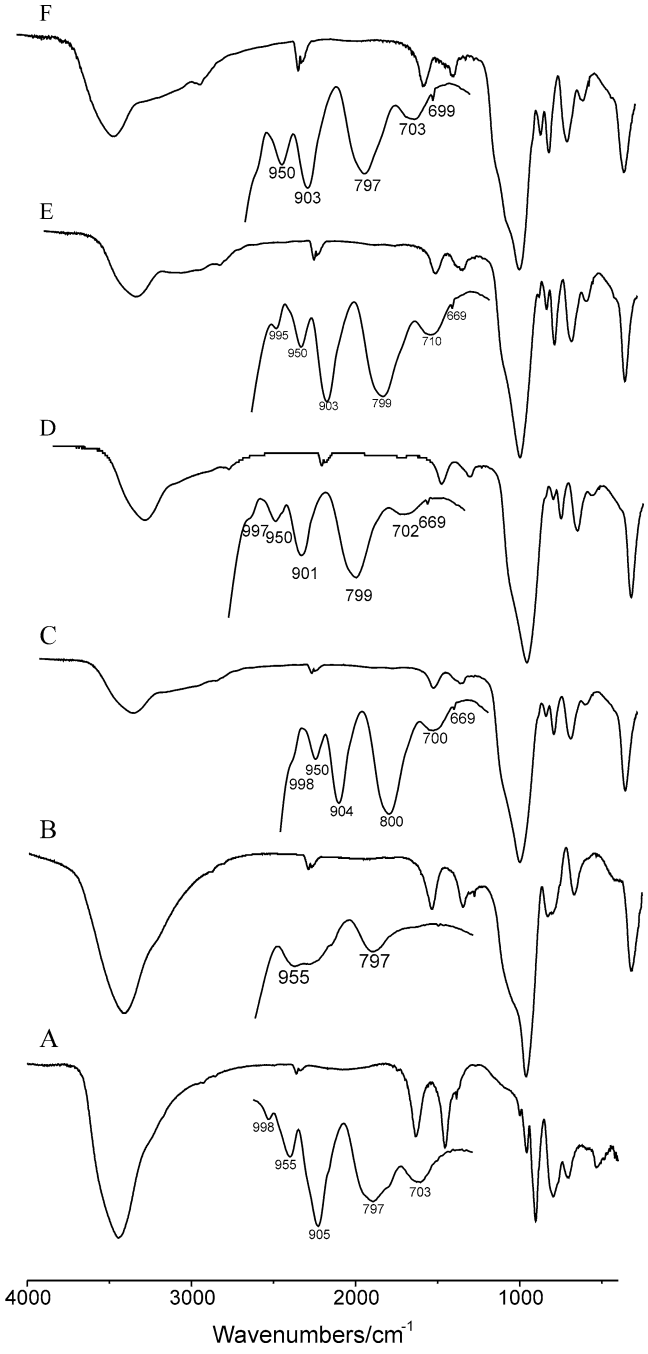

Fig. 2. FT-IR spectra of the starting $SiW_{11}Ni$ and their corresponding porous materials, (A) 1-$SiW_{11}Ni$; (B) microporous $SiW_{11}Ni/SiO_2$; (C) mesoporous $SiW_{11}Ni$–APS–SIO-5; (D) mesoporous $SiW_{11}Ni$–APS–SIO-6; (E) mesoporous $SiW_{11}Ni$–APS–SIO-7; (F) macroporous $SiW_{11}Ni$–APS–SiO_2. Inset: magnified FT-IR spectra of the composites in the range of 700 to 1050 cm^{-1}.

tion of N–H. . .O–H hydrogen bonding interactions. In theses composites, propylamine groups link to the silica surface through one or two Si–O–Si linkages, corresponding to stretching vibrations in the range of 1080 to 1106 cm^{-1}. These IR data also confirmed that the $SiW_{11}Ni$ cluster was attached onto the silica surface. That is, the stretching vibration bands of the $SiW_{11}Ni$-containing composites at W=O and W–O–W bonds still maintain the main characteristic of the $SiW_{11}Ni$ precursor. Some shifts of the wavenumbers at W–O–W bonds were attributed to interaction of $SiW_{11}Ni$ cluster with the amine-modified silica surface. The absorption peak (998 cm^{-1}) due to the central SiO_4 unit of the $SiW_{11}Ni$ cluster was impacted by the broad and intense peak due to the Si–O (1080 cm^{-1}) bond of the silica support, resulting in a decrease of the peak intensity. Interestingly, in comparison to the starting $SiW_{11}Ni$ or microporous $SiW_{11}Ni/SiO_2$, we found a new peak (weak but sharp) that appeared at 699 cm^{-1} in each of the $SiW_{11}Ni$–APS–silica materials. This new peak corresponded to the vibration of Ni–N dative bonding [29], which was formed via coordination of nickel centers in the cluster with the nitrogen atom of amine surface groups in silica. Evidence in confirmation of the presence of the Si–O bond from the central SiO_4 of $SiW_{11}Ni$ in the composites were ^{29}Si MAS NMR, i.e., chemical shift (δ) at -94.1 ppm (for $SiW_{11}Ni$–APS–SiO_2) originated from the central SiO_4 unit of $SiW_{11}Ni$ clusters, similar to that of the parent $SiW_{11}Ni$ (δ -93.0 ppm), suggesting that the Si–O bond in the central SiO_4 of $SiW_{11}Ni$ existed in the hybrid materials. Perturbation of the Si chemical environment was also attributed to the stronger interaction between the $SiW_{11}Ni$ molecule and the amine-modified silica support. The rest of the resonance signals were originated from Q^4 ($Si(OSi)_4$, δ 122.31 ppm), Q^3 ($Si(OSi)_3(OH)$, δ -116.44 ppm), Q^2 ($Si(OSi)_2(OH)_2$, δ -112.17 ppm), and Q^1 ($Si(OSi)(OH)_3$, δ -101.51 ppm), respectively, indicating that surface silanol groups existed in the hybrid materials.

The above spectroscopic observations are consistent with information derived from elemental analyses of the $SiW_{11}Ni$–APS–SiO_2(SIO) materials. We therefore conclude that in these materials the $SiW_{11}Ni$ clusters were chemically attached to the supports and their primary structure remained intact.

A series of impregnation experiments were performed to study the effects of the surface amine ligand and the Ni^{II} center. Both amine-modified and unmodified porous silica supports, and POM clusters with ($SiW_{11}Ni$) and without ($K_8SiW_{11}O_{39}$, SiW_{11}) Ni^{II} centers, were used, indicating that only $SiW_{11}Ni$–APS–SiO_2 resulted in the highest cluster retention after washing the composite with hot water (80 °C) for three times. This result indicated that chemical interactions existed in the $SiW_{11}Ni$–APS–SiO_2 composites. In cases of SiW_{11}–APS–SiO_2 and $SiW_{11}Ni$–SiO_2 (prepared by mixing the cluster and the supports at pH 6–7), $SiW_{11}Ni$ or SiW_{11} could be introduced to the surface of the support at loadings similar to those of the $SiW_{11}Ni$–APS–SiO_2. However, the clusters were completely removed after washing with water, as confirmed by ICP-AES analysis (the content of W in the composites was lower than 0.1%) and DR-UV–vis spectroscopy (no characteristic absorption peaks of the cluster). This result is due to electrostatic interactions between the cluster and the supports.

The physisorption of N_2 was studied to characterize the porosity of $SiW_{11}Ni$–APS–SiO_2(SIO) and $SiW_{11}Ni/SiO_2$

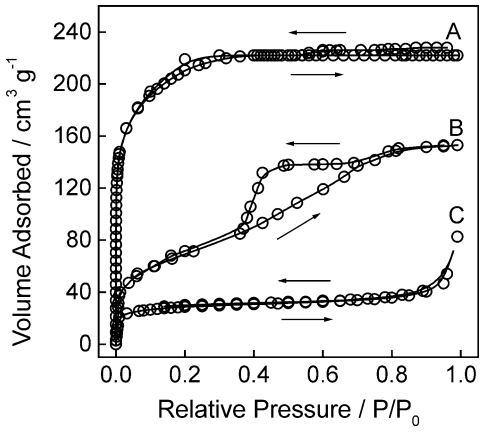

Fig. 3. Plots of nitrogen adsorption-desorption isotherms for micro-, meso-, and macroporous $SiW_{11}Ni$-containing silica materials. "→" refers to the adsorption branch, and "←" refers to the desorption branch.

materials. The resulting N_2 adsorption-desorption isotherms are shown in Fig. 3. The isotherms of microporous $SiW_{11}Ni/SiO_2$ and macroporous $SiW_{11}Ni$–APS–SiO_2 showed little or no hysteresis, which is indicative of microporosity and cylindrical pore geometries, and are type I in the IUPAC classification [30]. As for the mesoporous $SiW_{11}Ni$–APS–SiO_2(SIO) (represented by $SiW_{11}Ni$–APS–SiO_2), their isotherms belong to type IV, in which a hysteresis was observed for the desorption branch. It must be addressed that the microporosity of the macroporous $SiW_{11}Ni$–APS–SiO_2 determined by nitrogen adsorption refers to the porosity of its wall structure. The pore volume for the wall of macroporous $SiW_{11}Ni$–APS–SiO_2 materials was smaller, suggesting that only part of the micropores existed in the $SiW_{11}Ni$–APS–SiO_2 wall. This low pore volume of the wall may be due to crowding of the large Keggin units (1.0 nm) in the wall, which blocked part of the pores of the silica network. The calculated BET surface areas, pore volume, and average pore diameters based on the Barrett–Joyner–Halenda (BJH) method are summarized in Table 2. It shows that BET surface areas of the composites are higher than those of the pure $SW_{11}Ni$ (< 10 m^2/g). However, compared with the porous silica supports, both the BET surface area and the pore volume of the meso- and macroporous $SiW_{11}Ni$–APS–SiO_2(SIO) are reduced due to the introduction of organic groups and $SiW_{11}Ni$ clusters. The explanation for this result was that attachment of the cluster to an APS ligand extending into the pore channel would decrease the pore opening, thus effectively blocking other clusters from entering that channel. This would reduce the surface area accessible to $SiW_{11}Ni$ clusters.

The topologies of the composites were evaluated by TEM and/or SEM observations, and the results are shown in Fig. 4. For microporous $SiW_{11}Ni/SiO_2$, its SEM images showed that their particles were well distributed, and their average particle size was ca. 20 nm. However, from this SEM image we cannot find the micropores in the composites due to the limitation of resolution of the scanning electron microscope used, as well as serious aggregation of the particles. The TEM image of the mesoporous $SiW_{11}Ni$–APS–SiO_2(SIO) showed that the arrangement of the particles was uniform, and they exhibited lamellar structures; i.e., the center of the images showed aggregation of the particles, while the edges exhibited obvious porous structures. However, the exact analysis of the pore sizes and thickness of the pore walls for mesoporous $SiW_{11}Ni$-containing composites is difficult owing to heavy overlapping of the images. The estimated particle size for mesoporous $SiW_{11}Ni$–APS–SiO_2, $SiW_{11}Ni$–APS–SIO-5, $SiW_{11}Ni$–APS–SIO-6, and $SiW_{11}Ni$–APS–SIO-7 was 5, 20, 33, and 55 nm, respectively. In the case of macroporous $SiW_{11}Ni$–APS–SiO_2, both the SEM and TEM images showed that its structure was three-dimensional, and its particle size, pore size, and wall thickness was ca. 440, 380, and 60 nm, respectively.

3.2. Photocatalytic testing

3.2.1. Activity

The heterogeneous photocatalytic activities of the porous $SiW_{11}Ni/SiO_2$ and $SiW_{11}Ni$–APS–SiO_2(SIO) were tested by studying the degradation and mineralization of an aqueous RB compound. The disappearance of RB was monitored by UV–vis spectrometry at a wavelength of 554 nm. On stirring the suspension of aqueous RB solution (50 mg L^{-1} or 0.10 mmol L^{-1}) and the catalyst powder (containing 30 mg of pure $SiW_{11}Ni$ in each of $SiW_{11}Ni$-impregnated silica composites and the starting cluster) in the dark for 180 min, the disappearance of RB was negligible. In the absence of the catalyst, the disappearance of RB required ca. 600 min by direct photocatalysis. However, the UV irradiation time for RB degradation was shortened to different degrees when various porous $SiW_{11}Ni$-containing silica materials were used in this photocatalytic process, see Fig. 5. This result indicated that the charge transfer excited state of the anchored $SiW_{11}Ni$ species played a significant role in the photocatalyzed RB degradation. Moreover, the activity of the supported $SiW_{11}Ni$ was higher than that of pure $SiW_{11}Ni$ (i.e., RB was photodegraded in homogeneous system, see Fig. 5A). The above results are due to the porous structures of the catalysts, which allowed the photocatalytic reaction to perform in their pores, as if the catalysts were concentrated. Moreover, from the observed activity order for RB degradation we see that the photocatalytic activities of the porous composites mainly depended on their BET surface areas.

3.2.2. Mineralization

Total degradation of RB leads to the conversion of organic carbon into gaseous CO_2, whereas nitrogen is converted into ammonium ions and subsequent nitrate ions, the latter being the highest stable oxidation state of nitrogen (+5). In the present work, NH_4^+ and NO_3^- ions were detected during the photocatalytic degradation of aqueous RB on the porous $SiW_{11}Ni$-containing silica materials. The yield of NO_3^- ions reached 74.2% after 10 h of

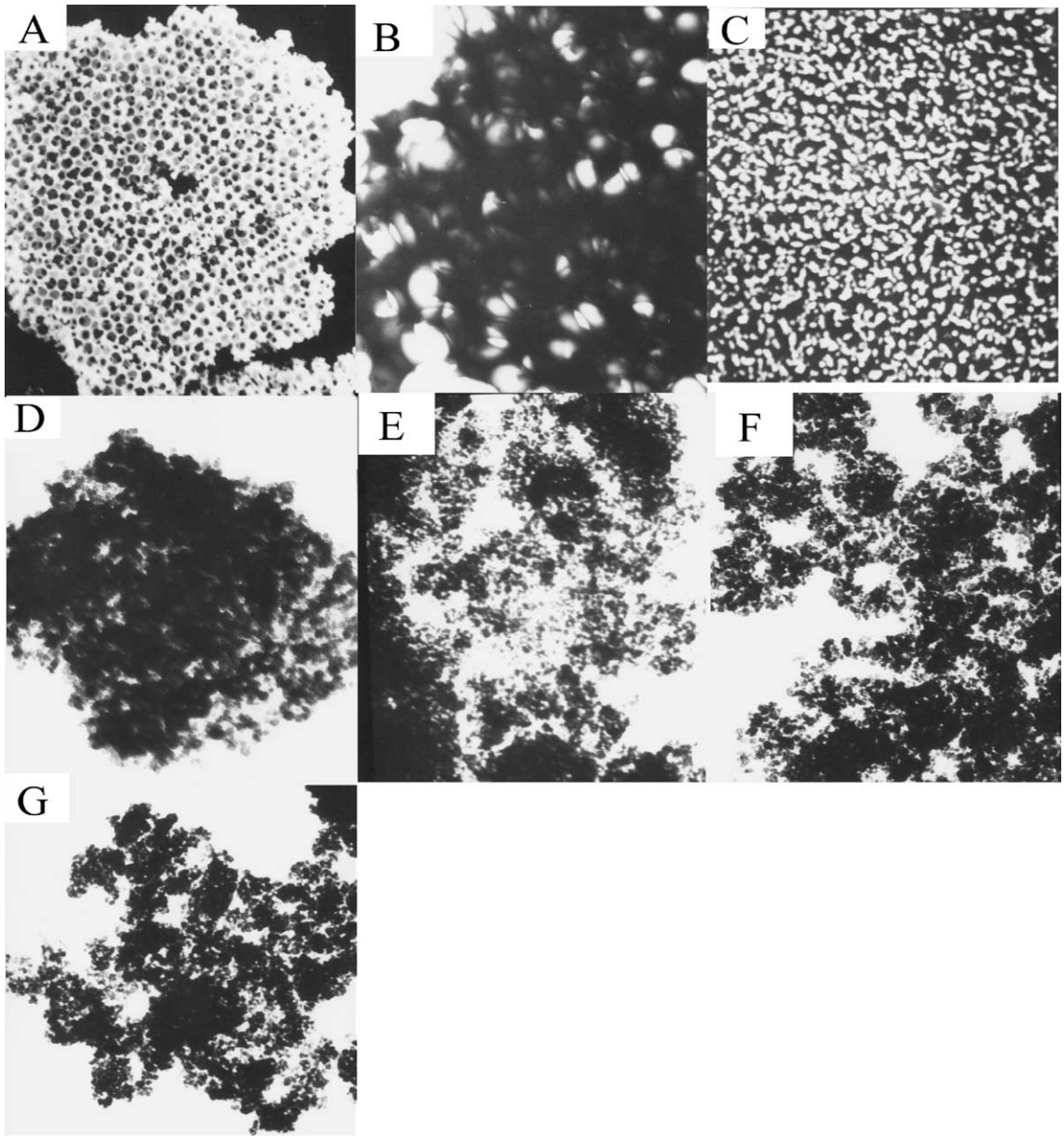

Fig. 4. SEM images of macroporous $SiW_{11}Ni$–APS–SiO_2, magnification 8000; (B) TEM images of macroporous $SiW_{11}Ni$–APS–SiO_2, magnification 20,000; (C) SEM images of microporous $SiW_{11}Ni/SiO_2$, magnification 10,000; (D) TEM images of mesoporous $SiW_{11}Ni$–APS–SiO_2, magnification 30,000; (E) TEM images of mesoporous $SiW_{11}Ni$–APS–SIO-5, magnification 40,000; (F) TEM images of mesoporous $SiW_{11}Ni$–APS–SIO-6, magnification 30,000; (G) TEM images of mesoporous $SiW_{11}Ni$–APS–SIO-7, 30,000.

UV irradiation (Fig. 6), and its concentration remained unchanged with the increasing irradiation time. Lower yields of NO_3^- ions may be due to the physical adsorption of NO_3^- ions at the surface of the porous photocatalysts.

3.2.3. Kinetics

The influence of the initial RB concentration (C_0) on the initial RB rates (r_0) for photocatalytic degradation of RB was studied, and the results are shown in Fig. 7. Via changing C_0 in the range of 0 to 50 mg L^{-1}, the plots of r_0 vs C_0 exhibited a nearly straight line, and the determined reaction rate constant (k) was 0.056, 0.043, and 0.035 min^{-1}, respectively, for microporous $SiW_{11}Ni/SiO_2$, mesoporous $SiW_{11}Ni$–APS–SiO_2, and macroporous $SiW_{11}Ni$–APS–SiO_2. The value of k for microporous $SiW_{11}Ni/SiO_2$ is the largest, and it is the smallest for macroporous $SiW_{11}Ni$–APS–SiO_2, suggesting that the rate of disappearance of RB in the presence of the supported $SiW_{11}Ni$ depends on the specific surface areas of the catalysts used.

The above first-order linear relationship can be explained in a Langmuir–Hinshelwood model

$$r = \frac{-\mathrm{d}C}{\mathrm{d}t} = \frac{-kKC}{(1+KC)}. \quad (1)$$

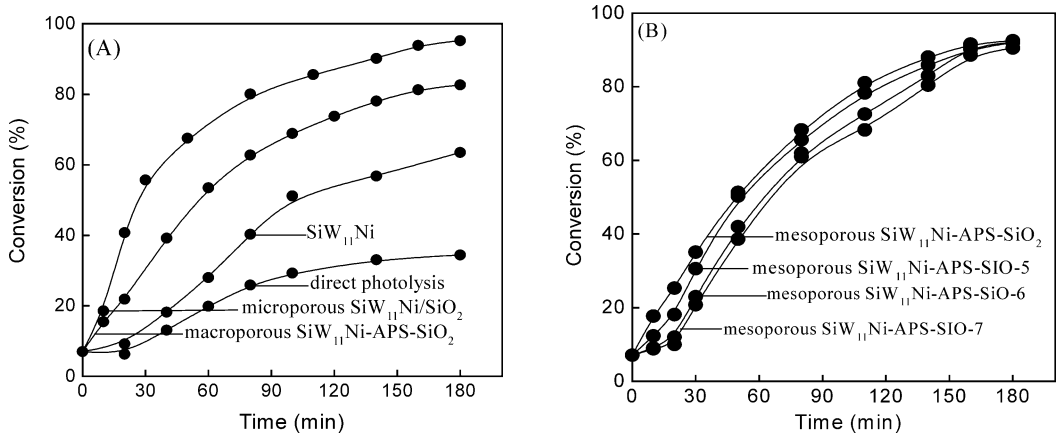

Fig. 5. Disappearance of RB ($C_0 = 50$ mg L^{-1} or 0.10 mmol L^{-1}) over the various supported SiWiiNi. In each of the composites, the content of pure $SiW_{11}Ni$ was 30 mg.

As for the dilute solution, $KC \ll 1$ (K refers to the adsorption equilibrium constant) because of the weak adsorption of RB on the surface of the catalyst, the above model can be expressed by

$$r = kKC. \tag{2}$$

Therefore, the reaction of the photocatalytic degradation of RB by the supported $SiW_{11}Ni$ is apparent first-order kinetics of a Langmuir–Hinshelwood model, whose apparent relationships are due to the low concentration of RB chosen.

3.2.4. Mechanism

IC together with ES-MS detected 13 intermediates (see Scheme 3) generated during the RB degradation process. We therefore proposed the mechanism of photocatalytic degradation of RB over the porous $SiW_{11}Ni$-containing silica composites.

At first, the reactants (RB and dioxygen) reached the surface and entered into the pores of the composites through diffusion, and then they were adsorbed on the surface and in the pores by a hydrogen bonding interaction between carboxy groups of RB and surface hydroxyl groups of silica supports, where they were accessible to the active sites (W–O–W bonds) anchored within the pore cavities. This adsorption reached equilibrium after the suspension was stirred for 30 min, and conversion of RB was 7.8%.

Second, the catalysts were photonactivited by UV irradiation and initiated the RB degradation reaction [31–34]. That is, UV irradiation of the polyoxotungstate cluster results in the charge transfer from an O^{2-} ion to a W^{6+} ion occurring at W–O–W bonds, leading to the formation of a pair of a hole center (O^-) and a trapped electron center (W^{5+}):

$$\left[W^{6+}\text{–}O^{2-}\text{–}W^{6+}\right] \xrightarrow{h\nu} \left[W^{5+}\text{–}O^{-}\text{–}W^{6+}\right]^{*}. \tag{3}$$

The HOMO-LUMO energy gap for the Keggin units is 4.5 eV. The charge transfer-excited state of POM, $[W^{5+}$–O–$W^{6+}]^*$, has strong oxidation ability, and is responsible for oxidation of RB in the inorganic products.

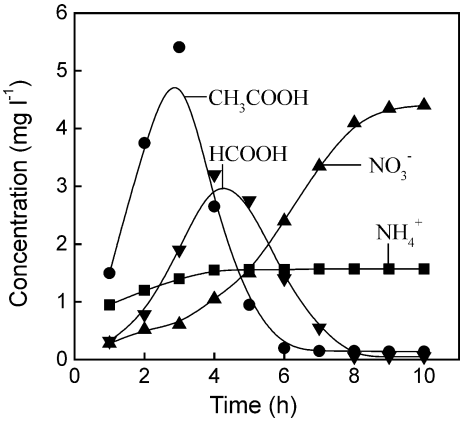

Fig. 6. Evolution of acetic acid, formic acid, ammonium ions, and nitrate ions in the solution during photocatalytic degradation of RB ($C_0 = 50$ mg L^{-1}) on the mesoporous $SiW_{11}Ni$–APS–SiO_2 (containing 30 mg of pure $SiW_{11}Ni$) composite.

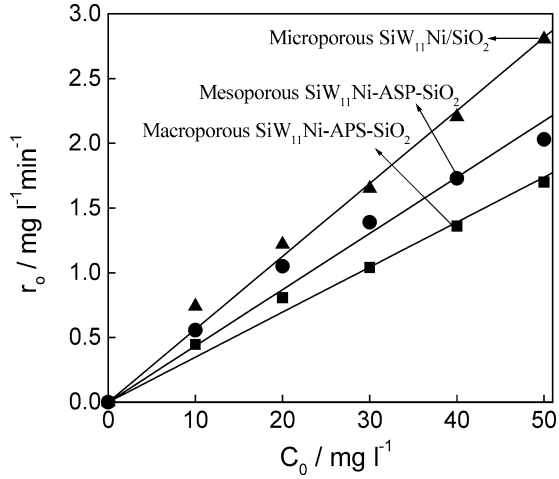

Fig. 7. Variations of the initial RB degradation rates (r_0) as a function of the RB initial concentrations (C_0).

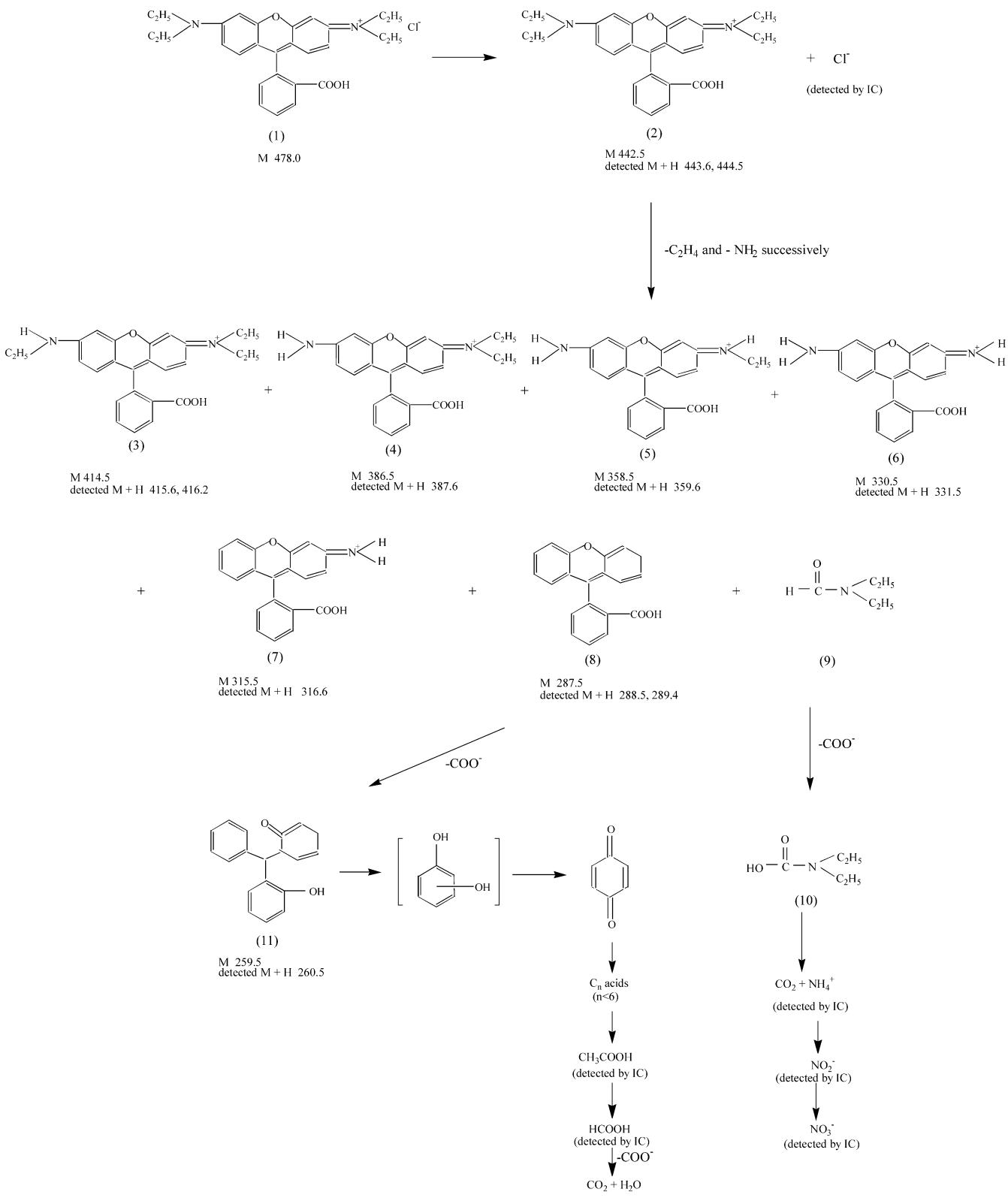

Scheme 3. Pathway of the photocatalytic degradation of aqueous RB on the amine-modified silica impregnated by $SiW_{11}Ni$. M, molecular weight.

According to the above discussion and the identified intermediates, an aqueous RB may be degraded following the two steps:

(i) Photooxidation of RB via successive attacks by $OH^{\cdot}$ radicals, and $OH^{\cdot}$ radicals were produced by neutralization of OH^- groups with a hole center (O^-),

$$O^- + H_2O \ (\Leftrightarrow H^+ + OH^-) \rightarrow OH^{\cdot} + H_2O, \quad (4)$$

$$RB + OH^{\cdot} \rightarrow RB' + H_2O; \quad (5)$$

here RB′ refers to the products of RB deethylation and deamination (Compounds 3–8 in Scheme 3);

(ii) Decarboxylation from the intermediates (Compounds 8 and 9, and formic acid), resulting in Compounds 10, 11, and final product CO_2 via direct reaction with holes (O^-). This is the so-called photo-Kolbe reaction,

$$RCOO^- + O^- \rightarrow R'' + CO_2, \quad (6)$$

where R″ refers to Compounds 10, 11, and final product CO_2.

Continuing UV irradiation resulted in total cleavage of the RB chromophore into polyphenol and quinone, and decolorization of RB was finalized (the reaction solution was colorless at this time). However, the disappearance of RB does not mean its total degradation. It required a reaction time longer than that for destruction of its chromophore due to the successive cleavage of carbon chain. From Fig. 6 we observed that disappearance of the intermediates such as acetic acid and formic acid required 360 and 480 min, respectively.

After the reactions finished, the suspensions were centrifuged, and the catalysts (mesoporous $SiW_{11}Ni$–APS–SIO-5-7 and macroporous $SiW_{11}Ni$–APS–SiO_2) were separated. The concentration of W in each clear reaction solution was determined by ICP-AES, and it was 1.6, 1.9, 2.2, 3.0, and 3.2 mg L^{-1}, respectively. (The original content of W was 225 mg L^{-1}.) Thus, the decreased percentage of W into the reaction system was in the range of 0.7 to 1.4%. This result confirmed that the $SiW_{11}Ni$ molecule and the amine-modified silica support were combined via chemical interaction in the as-synthesized composites, and the dropped cluster may be interacted with the support by physical adsorption.

4. Conclusions

Mesoporous and macroporous amine-modified silica materials based on monosubstituted Keggin units [$SiW_{11}Ni$] were prepared through coordination of nickel centers in the $SiW_{11}Ni$ cluster with the nitrogen atom of amine surface groups in propylamine-modified silica supports. Spectroscopic and elemental analysis data showed that the $SiW_{11}Ni$ clusters were attached to the silica supports via Ni–N dative bonding, and that the primary Keggin structure of $SiW_{11}Ni$ remained intact in the as-synthesized materials. Some shifts of IR absorption peaks at W–O–W bonds and perturbation of the Si chemical environment were attributed to the coordination interaction of the $SiW_{11}Ni$ cluster with the amine-modified silica surface. Compared with the $SiW_{11}Ni$ in homogeneous systems, the photocatalytic activity of $SiW_{11}Ni$-containing hybrid catalysts has been improved due to their pore structure. In addition, the leaching of $SiW_{11}Ni$ from the support was controlled effectively due to the chemical attachment of the cluster onto the support.

The major advantage of the supported $SiW_{11}Ni$ over homogeneous $SiW_{11}Ni$ was not their reactivity but the ease in separation and recovery of the solids containing highly dispersed clusters, and minor clusters leached into the reaction system during the reaction.

Acknowledgments

The Natural Science Fund Council of China is acknowledged for financial support (No.20071007). The present work is also supported by the Foundation for University Key Teacher by the Ministry of Education of China.

References

[1] M.T. Pope, A. Müller, Angew. Chem. Int. Ed. Engl. 30 (1991) 34.
[2] Y.A. Vlasov, N. Yao, D.J. Norris, Adv. Mater. 11 (1999) 165.
[3] N. Mizuno, M. Misono, Chem. Rev. 98 (1998) 199.
[4] I.V. Kozhevnikov, Chem. Rev. 98 (1998) 171.
[5] D.E. Katsoulis, Chem. Rev. 98 (1998) 359.
[6] T. Okuhara, T. Nishimura, H. Watanabe, M. Misono, Stud. Surf. Sci. Catal. 90 (1994) 419.
[7] K.Y. Lee, T. Arai, S. Nakata, S. Asaoka, T. Okuhara, M. Misono, J. Am. Chem. Soc. 114 (1992) 2863.
[8] Y. Izumi, M. Ono, M. Kitagawa, M. Yoshida, K. Urabe, Micropor. Mater. 5 (1995) 255.
[9] Y. Guo, C. Hu, Y. Wang, E. Wang, Y. Zhou, S. Feng, Chem. Mater. 12 (2000) 3501.
[10] Y. Guo, C. Hu, X. Wang, E. Wang, Y. Zhou, S. Feng, Chem. Mater. 13 (2001) 4058.
[11] Y. Guo, Y. Yang, C. Hu, C. Guo, E. Wang, Y. Zhou, S. Feng, J. Mater. Chem. 12 (2002) 3046.
[12] A.P. Wight, M.E. Davis, Chem. Rev. 102 (2002) 3589.
[13] R. Neumann, C.J. Abu-Gnim, Chem. Soc., Chem. Commun. (1989) 1324.
[14] R. Neumann, C. Abu-Gnim, J. Am. Chem. Soc. 112 (1990) 6025.
[15] N. Mizuno, M. Tateishi, T. Hirose, M. Iwamoto, Chem. Lett. (1993) 1985.
[16] N. Mizuno, T. Hirose, M. Tateishi, M. Iwamoto, Chem. Lett. (1993) 1839.
[17] C. Hu, M. Hashimoto, T. Okuhara, M. Misono, J. Catal. 143 (1993) 437.
[18] A.M. Khenkin, C.L. Hill, J. Am. Chem. Soc. 115 (1993) 8178.
[19] L.C.W. Baker, J.S. Figgis, J. Am. Chem. Soc. 92 (1970) 3794.
[20] H.Y. Woo, H. So, M.T. Pope, J. Am. Chem. Soc. 118 (1996) 621.
[21] M. Vautier, C. Guillard, J.-M. Herrmann, J. Catal. 201 (2001) 46.
[22] C. Hu, Y. Wang, H. Tang, Appl. Catal. B 35 (2001) 95.
[23] J. Grzechulska, A.W. Morawski, Appl. Catal. B 36 (2002) 45.

[24] G. Liu, J. Zhao, New J. Chem. 24 (2000) 411.
[25] C.M. Tourne, G.F. Tourne, J. Inorg. Nucl. Chem. 32 (1970) 3975.
[26] J.W. De Hann, H.M. Van Den Bogaert, J.J. Ponjee, L.J.M. Van De Ven, J. Colloid Interface Sci. 110 (1986) 519.
[27] K. Moller, T. Bein, Chem. Mater. 10 (1998) 2950.
[28] M.T. Pope, Heteropoly and Isopoly Oxometalates, Springer, Berlin, 1983.
[29] Sadtler Research Laboratories Inc., Sadtler Commercial IR Grating Spectra, Inorganics, 1-2, Y271K, Y264K, Philadelphia, 1987.
[30] S.J. Gregg, K.S.W. Sing, Adsorption, Surface Area and Porosity, 2nd ed., Academic Press, London, 1995.
[31] Y. Guo, D. Li, C. Hu, Y. Wang, E. Wang, Y. Zhou, S. Feng, Appl. Catal. B 30 (2001) 337.
[32] Y. Guo, C. Hu, S. Jiang, C. Guo, Y. Yang, E. Wang, Appl. Catal. B 36 (2002) 9.
[33] D. Stattari, C.L. Hill, J. Am. Chem. Soc. 115 (1993) 4649.
[34] A. Mylonas, A. Hiskia, E. Androulaki, D. Dimotikali, E. Papaconstantinou, Phys. Chem. Chem. Phys. 1 (1999) 437.